

Enhancing Multi-modal Learning: Meta-learned Cross-modal Knowledge Distillation for Handling Missing Modalities

Hu Wang¹, Congbo Ma², Yuyuan Liu¹, Yuanhong Chen¹, Yu Tian³, Jodie Avery¹, Louise Hull¹, and Gustavo Carneiro⁴

¹ The University of Adelaide, Adelaide, Australia

² Macquarie University, Sydney, Australia

³ Harvard University, Massachusetts Hall, United States

⁴ University of Surrey, Guildford, United Kingdom

Abstract. In multi-modal learning, some modalities are more influential than others, and their absence can have a significant impact on classification/segmentation accuracy. Hence, an important research question is if it is possible for trained multi-modal models to have high accuracy even when influential modalities are absent from the input data. In this paper, we propose a novel approach called Meta-learned Cross-modal Knowledge Distillation (MCKD) to address this research question. MCKD adaptively estimates the importance weight of each modality through a meta-learning process. These dynamically learned modality importance weights are used in a pairwise cross-modal knowledge distillation process to transfer the knowledge from the modalities with higher importance weight to the modalities with lower importance weight. This cross-modal knowledge distillation produces a highly accurate model even with the absence of influential modalities. Differently from previous methods in the field, our approach is designed to work in multiple tasks (e.g., segmentation and classification) with minimal adaptation. Experimental results on the Brain tumor Segmentation Dataset 2018 (BraTS2018) and the Audiovision-MNIST classification dataset demonstrate the superiority of MCKD over current state-of-the-art models. Particularly in BraTS2018, we achieve substantial improvements of 3.51% for enhancing tumor, 2.19% for tumor core, and 1.14% for the whole tumor in terms of average segmentation Dice score.

Keywords: Multi-modal Learning · Missing Modalities · Meta-learning · Cross-modal Knowledge Distillation

1 Introduction

Multi-modal learning is a technique that builds classification/segmentation models that integrate and process information from multiple data modalities (e.g., text, images, audio, video, sensor data, etc.). The goal of multi-modal learning is to leverage the complementary information provided by different modalities

to enhance task performance when compared with each modality in isolation. Multi-modal learning has been explored in many fields, such as computer vision (CV) and medical image analysis (MIA), and applications, like autonomous driving [33], robot navigation [39], general multi-modal dialog system [30], and medical multi-modal diagnosis [40]. However, a common challenge in multi-modal learning is how to handle input data when a subset of the input modalities are missing since the models mentioned above generally require all modalities to always be present.

The challenge presented by multi-modal learning with missing modalities has attracted significant interest. In CV, the learning of a shared multi-modal space to handle incomplete and unlabeled multi-view data [44] can address this challenge. Ma et al. [25] introduced the model SMIL, trained with meta-learning to address multi-modal learning with missing modalities. In MIA, several models [10, 14] attempted to adopt statistical features (mean and variance) as embeddings for the model’s decoding process for dealing with missing modalities. Also, some methods [34, 42] approximate the missing features using all modalities. The work [42] further introduced a “dedicated” training strategy, optimizing independent but related models for each missing modality situation. Relying on a different strategy, the methods in [7, 38] proposed feature disentanglement models, aiming to separate modality-shared features and modality-specific features to better tackle missing modalities. A fact in multi-modal learning is that there are certain modalities that contribute more than others for a certain task – see Fig. 1. However, previous methods do not try to identify the most influential modalities in a multi-modal learning framework. Consequently they do not distill the knowledge from the more influential to the less influential modalities, which could be useful to enable high performance even when the most influential modalities are absent from the set of multi-modal testing images. Moreover, these methods are often designed to be task-specific (examples of tasks are classification or segmentation), so they cannot be easily adapted to work on multiple tasks with minimal adaptation.

In this paper, we propose a novel method, named **M**eta-learned **C**ross-modal **K**nowledge **D**istillation (MCKD), for multi-modal learning with missing modalities designed to handle the challenges mentioned above. MCKD automatically estimates the importance weights and distills useful knowledge from the “important” modalities using meta-learning. Also, MCKD is easily adaptable to multiple tasks (e.g., classification and segmentation). An intuitive visualization with modality-specific segmentations and learned importance weights are shown in Fig. 1, where the modality T1c has the highest importance weight and shows the most accurate segmentation, thus providing evidence for our motivation. Our main contributions are:

- An innovative multi-modal learning model named MCKD, which addresses the issue of missing modalities by leveraging a meta-learning approach to distill valuable knowledge from the modalities that show higher accuracy to the modalities with lower accuracy; and

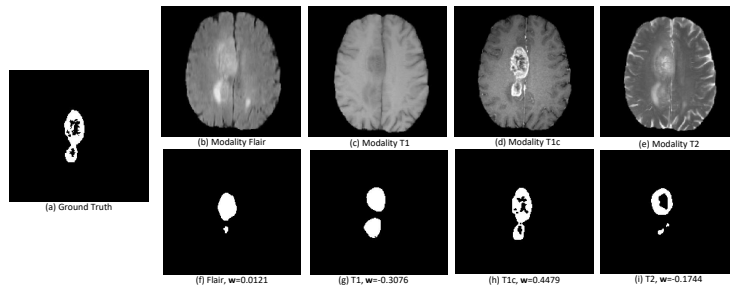


Fig. 1: Visualization of the enhancing tumor (ET) segmentation results from each modality on a BraTS2018 image. Sub-figure (a) shows the Ground Truth segmentation; (b)-(e) and (f)-(i) display the original modalities (Flair, T1, T1c or T2) and their segmentations, along with the importance weights (\mathbf{w} in the legend) learned automatically (before normalization) by our MCKD. Notice that the modality T1c has the highest importance weight for cross-modal knowledge distillation, and it also shows the most accurate segmentation, compared with the ground truth.

- A flexible model design that enables MCKD to easily adapt to multiple tasks, such as classification and segmentation.

Experimental results on medical imaging segmentation and computer vision classification benchmarks demonstrate that MCKD achieves state-of-the-art performance in multi-modal learning with missing modalities. Particularly when compared to recently proposed state-of-the-art methods on BraTS2018, our model exhibits remarkable segmentation accuracy, with improvements of 3.51% for enhancing tumor, 2.19% for tumor core, and 1.14% for the whole tumor.

2 Related Work

2.1 Multi-modal Learning

Multi-modal learning is increasingly important in a wide range of applications, such as medical image analysis, computer vision, natural language processing, and robotics, where data from different sources can provide a complementary and accurate understanding of the underlying task. In multi-modal learning, algorithms are designed to analyze and extract features from each modality, and then combine these features to make more informed decisions or predictions.

In medical image analysis (MIA), the work [11] introduced a chilopod-shaped architecture that was optimized using a modality-dependent feature normalization and a knowledge distillation objective, which only works effectively when all modalities are available in the input. In a different approach, the method based on pixel-wise coherency [28] has been developed for multi-modal learning by modeling aleatoric uncertainty in image segmentation with the generation of multiple hypotheses through joint distributions over label maps. Han et al. [13] designed a trusted multi-view classifier by modeling multi-modal uncertainties

using the Dirichlet distribution and fusing features through Dempster’s rule. Wang et al. [40] introduced an uncertainty-aware multi-modal learning model based on cross-modal random network prediction.

In computer vision (CV), channel exchanging and multi-modal learning were combined to fuse features effectively [41]. For video/audio classification and retrieval tasks, self-supervised learning was proposed [31, 32] to train multi-modal models on additional data, leading to large performance improvements. A model to enhance video-and-sound source localization accuracy was developed [8] by defining a trusted tri-map middle-ground. Jia et al. [16] introduced a model for multi-view learning by constraining the view-specific features to be orthogonal to the view-shared features. Feature disentanglement methods [18, 22] aim to model data variations by learning modular and informative representations.

The methods mentioned above show effective multi-modal learning results, but they assume that all modalities are always available in training and testing, limiting their applicability in real-world scenarios, where some of the input modalities may be missing during training and testing.

2.2 Multi-modal Learning with Missing Modalities

To address the issue of missing modalities in multi-modal learning, various methods have been developed [19–21, 24]. In MIA, the HeMIS model was developed [14] to learn modality-specific embeddings, allowing arithmetic operations (e.g., mean and variance) on these embeddings to produce segmentations. Dorent et al. [10] extended HeMIS with a multi-modal variational auto-encoder (MVAE) that produced pixel-wise classifications based on mean and variance features. Similarly, auto-encoder structures have been used for unsupervised learning of missing modalities [6, 36]. Several other approaches [15, 34, 42] proposed the learning of missing modality features from full modality models to enhance embeddings. Some papers [7, 38] proposed a feature disentanglement approach that aimed to learn modality-shared and modality-specific features for better performance. A vision transformer architecture [45] was introduced for multi-modal brain tumor segmentation, aiming to fuse features from all modalities into comprehensive representations.

In CV, the model in [44] aimed to learn a unified subspace to work with incomplete and unlabeled multi-view data. Albanie et al. [1] developed a cross-modal transfer model to transfer knowledge between modalities. However, it cannot learn the modality-importance automatically and only works for video-speech classification. There are also other works that attempted to handle missing modalities [2, 9, 43, 46], but they either can only be applied for segmentation task or merely work for a specific type of disease, which inevitably hampers the application of these models. Ma et al. [25] proposed the SMIL model, which employed a meta-learning algorithm to reconstruct features from missing modalities. Unlike SMIL, which uses meta-learning to handle missing modalities by updating two auxiliary networks, we apply meta-learning to train a set of modality importance weights for cross-modal knowledge distillation. Also, we

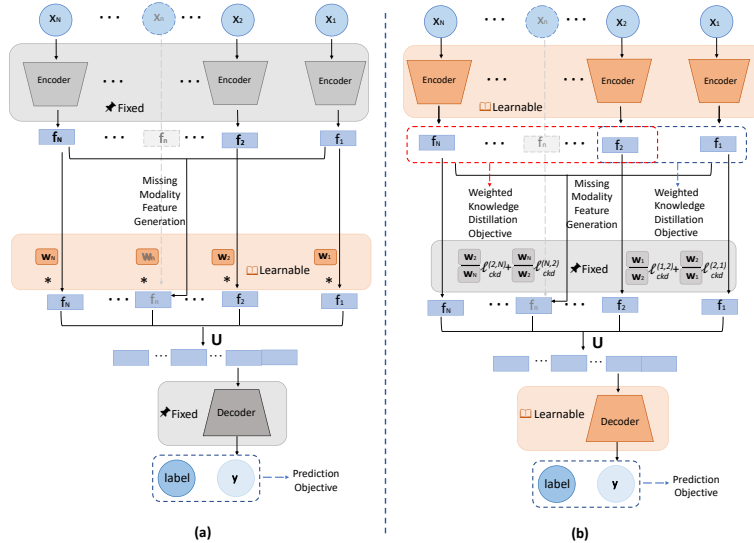


Fig. 2: MCKD model framework for (a) importance weight vector training and (b) main task and CKD training.

notice that in practice, SMIL has high memory complexity and exhibits unstable performance in missing modality scenarios.

Similarly to the multi-modal methods presented Sec. 2.1, existing missing modality methods are task-specific and do not readily adapt to both classification and segmentation tasks. More importantly, although these models are designed to handle missing modalities by reconstructing or fusing features, they neglect the fact that certain modalities perform better than others for classification or segmentation. It would be desirable to retain the performance produced by these “important” modalities, even when they are not present in training or testing. Our proposed MCKD aims to address the aforementioned weaknesses by automatically identifying and distilling the knowledge from influential modalities to dramatically enhance the model performance, particularly when such influential modalities are not present in the input data. MCKD is also designed to easily adapt to disparate (e.g., classification or segmentation) tasks.

3 Methodology

3.1 Model Structure

Let us denote the N -modality data as $\mathcal{M}_l = \{\mathbf{x}_i^l\}_{i=1}^N$, where $\mathbf{x}_i^l \in \mathcal{X}$ represents the l^{th} data sample and the subscript “ i ” indexes the modality. The corresponding label for each set \mathcal{M} is represented by $\mathbf{y}^l \in \mathcal{Y}$, where \mathcal{Y} denotes the ground-truth annotation space. To simplify the notation, we may omit the subscript l when the context is clear.

Our proposed MCKD, illustrated in Fig. 2, consists of a two-stage meta-learning method. The first stage estimates the importance weight for each modality when training for the task represented by the label \mathbf{y} (note that it is possible that a single dataset has multiple sub-tasks, such as the three types of tumor segmentation in the BraTS2018 dataset [3, 26]). This modality importance weight indicates the “amount” of knowledge contained in that modality. The second stage consists of multiple teacher-student training processes, along with the main task optimization (e.g. classification or segmentation), where for each pair of available modalities, we distill the knowledge from the teacher to the student using the ratio of their importance weights.

As illustrated in Fig. 2, each non-missing modality \mathbf{x}_i is fed into the encoder, parameterized by θ_i , which extracts the feature \mathbf{f}_i , with

$$\mathbf{f}_i = f_{\theta_i}(\mathbf{x}_i). \quad (1)$$

In order to simplify the model, the encoders’ parameters $\{\theta_i\}_{i=1}^N$ are shared among all modalities. For the missing modalities in Eq. (1), let us assume that the modalities in $\mathcal{Q} \subset \mathcal{M}$ are unavailable (i.e., all $\mathbf{x}_n \in \mathcal{Q}$ are represented by $\mathbf{x}_n = \emptyset$), then the missing features from those modalities can be generated based on the available features, as follows:

$$\mathbf{f}_n = \frac{1}{N - |\mathcal{Q}|} \sum_{\mathbf{x}_i \in \mathcal{M} \setminus \mathcal{Q}} f_{\theta_i}(\mathbf{x}_i) \quad (2)$$

for all $\mathbf{x}_n \in \mathcal{Q}$, with \setminus denoting the set subtraction operator.

The features obtained from Eq. (1) or generated from Eq. (2) are concatenated and fed into the decoder, parameterized by ζ , to make predictions, as in:

$$\hat{\mathbf{y}} = f_{\zeta} \left(\oplus_{i=1}^N \mathbf{f}_i \right), \quad (3)$$

where $\hat{\mathbf{y}}$ is the prediction, and $\oplus_{i=1}^N$ is the concatenator operator of the N extracted features.

3.2 Knowledge Distillation Meta-learning

We formulate the training of MCKD with a meta-learning bi-level optimization that contains a meta-parameter represented by an **importance weight vector (IWV)** $\mathbf{w} = [\mathbf{w}_1, \dots, \mathbf{w}_N]^T \in \mathbb{R}^N$. The inner learning uses the training set $\mathcal{D}_t = \{(\mathcal{M}, \mathbf{y})^l\}_{l=1}^{|\mathcal{D}_t|}$ to optimize the parameters of the model responsible to realize the main task of interest (e.g., classification or segmentation), while the meta-parameters are estimated from the outer learning that optimizes a meta-objective with a validation set $\mathcal{D}_v = \{(\mathcal{M}, \mathbf{y})^l\}_{l=1}^{|\mathcal{D}_v|}$ (where $\mathcal{D}_t \cap \mathcal{D}_v = \emptyset$), as in:

$$\begin{aligned} \mathbf{w}^* &= \arg \min_{\mathbf{w}} \sum_{(\mathcal{M}, \mathbf{y}) \in \mathcal{D}_v} \ell_{meta} \left(\mathbf{y}, f_{\zeta^*} \left(\oplus_{i=1}^N \mathbf{w}_i \times \mathbf{f}_i^* \right) \right) \\ \text{s.t. } \theta^*, \zeta^* &= \arg \min_{\theta, \zeta} \sum_{(\mathcal{M}, \mathbf{y}) \in \mathcal{D}_t} \left[\ell_{task} \left(\mathbf{y}, f_{\zeta} \left(\oplus_{i=1}^N \mathbf{f}_i \right) \right) + \alpha \sum_{i,j=1}^N \frac{\mathbf{w}_i^*}{\mathbf{w}_j^*} \times \ell_{ckd}^{(i,j)} (\mathbf{f}_i, \mathbf{f}_j) \right], \end{aligned} \quad (4)$$

where $\mathbf{f}_i^* = f_{\theta_i^*}(\mathbf{x}_i)$ or computed with (2) (similarly for $\mathbf{f}_i = f_{\theta_i}(\mathbf{x}_i)$), θ and ζ are the learnable parameters of the model encoder and decoder, respectively, the loss functions $\ell_{meta}(\cdot)$ and $\ell_{task}(\cdot)$ are represented by the element-wise (pixel in 2D or voxel in 3D) cross-entropy loss plus Dice loss for segmentation and the cross-entropy loss for classification. Also in Eq. (4), we have the **cross-modal knowledge distillation (CKD)** loss defined as

$$\ell_{ckd}(\mathbf{f}_i, \mathbf{f}_j) = \delta(\mathbf{x}_i \neq \emptyset) \times \delta(\mathbf{x}_j \neq \emptyset) \times \|\mathbf{f}_i - \mathbf{f}_j\|_p, \quad (5)$$

which is the p -norm of the difference between the encoder features of modalities $i, j \in \{1, \dots, N\}$ (with $\delta(\mathbf{x}_i \neq \emptyset)$ indicating that the modality i is present), with α being the trade-off factor between the $\ell_{task}(\cdot)$ and $\ell_{ckd}(\cdot)$ to balance the contribution of both losses to the CKD objective, and $\frac{\mathbf{w}_i^*}{\mathbf{w}_j^*}$ denoting the cost to penalize feature differences particularly with respect to the features from the modalities with large IWV. If we use ReLU or sigmoid normalization for each element within IWV, the elements lose connection with each other as ReLU or sigmoid do not take all elements into consideration, which will in turn affect the gradient back-propagation. The influences of different normalization methods on model performance can be found in the Supplementary Material. Thus, we normalize the IWV weight vector with a softmax activation function which provides the best performance by keeping the relative importance of the modalities, with

$$\mathbf{w}_i \leftarrow e^{\mathbf{w}_i} \div \left(\sum_{j=1}^N e^{\mathbf{w}_j} \right), \quad \text{for } i = 1, \dots, N, \quad (6)$$

updated at each iteration of the optimization in Eq. (4). This knowledge distillation between pairs of teachers and students leads to a convergence of features to be similar to the features from the modalities with greater weight in the IWV. Additionally, note that such pairwise knowledge distillation allows each modality to act as teachers to other modalities (with different importance weights), resulting in the distillation of knowledge from potentially many modalities through this dynamical process. The MCKD training is presented in Algorithm 1.

4 Experiments

4.1 Datasets

We evaluate the effectiveness of our MCKD model to deal with multi-modal learning with missing modality on two datasets: BraTS2018 for medical image segmentation, and Audiovision-MNIST for computer vision classification.

The BraTS2018 Segmentation Challenge dataset [3, 26] serves as our benchmark for multi-modal learning with missing modality in brain tumor sub-region segmentation. The dataset consists of 3D multi-modal brain MRIs, including Flair, T1, T1 contrast-enhanced (T1c), and T2 images, each annotated by experienced imaging experts to provide ground-truth segmentation of specific sub-regions, namely, enhancing tumor (ET), tumor core (TC), and whole tumor

Algorithm 1: Meta-learned Cross-modal Knowledge Distillation Framework.

Input: Multi-modal with missing modality dataset for meta-training and meta-validation $\mathcal{D} = \{\mathcal{D}_t, \mathcal{D}_v\}$, encoder and decoder, # iterations= N

Output: Encoder and decoder parameters θ^* and ζ^*

Initialize model parameters θ and ζ and meta-parameter \mathbf{w}

while *not converged* **do**

Meta-validation & Meta-updating:

$\mathbf{w}^* = \arg \min_{\mathbf{w}} \sum_{(\mathcal{M}, \mathbf{y}) \in \mathcal{D}_v} \ell_{meta}(\mathbf{y}, f_{\zeta}(\oplus_{i=1}^N \mathbf{w}_i \times \mathbf{f}_i))$

 Normalize \mathbf{w}^* with Eq. (6)

Meta-training:

for $n=1$ to N **do**

 Optimize task and CKD objectives:

$\theta^*, \zeta^* = \arg \min_{\theta, \zeta} \sum_{(\mathcal{M}, \mathbf{y}) \in \mathcal{D}_t} [\ell_{task}(\mathbf{y}, f_{\zeta}(\oplus_{i=1}^N \mathbf{f}_i)) + \alpha \sum_{i,j=1}^N \frac{\mathbf{w}_i^*}{\mathbf{w}_j^*} \times \ell_{ckd}^{(i,j)}(\mathbf{f}_i, \mathbf{f}_j)]$

end

$\theta \leftarrow \theta^*, \zeta \leftarrow \zeta^*$

end

(WT). The BraTS2018 dataset is composed of 285 cases for training, comprising 210 high-grade gliomas and 75 low-grade gliomas, and an additional 66 cases for evaluation. While the ground-truth annotations for the training set are publicly available, the annotations for the validation set have not been disclosed. Thus, we conducted an online evaluation⁵ using the hidden validation annotations to ensure an unbiased and objective assessment.

Our missing modality experiments for computer vision classification are conducted on the Audiovision-MNIST dataset [37]. This dataset presents a unique multi-modal combination of audio and image files, comprising a total of 1500 samples. The image samples represent digits 0 to 9 and have a dimension of 28×28 , originating from the well-known MNIST dataset [17]. The audio segment of the dataset consists of 1500 audio files, sourced from the Free Spoken Digits Dataset⁶. Following the settings of SMIL⁷ [25], to represent the audio modality effectively, we employ mel-frequency cepstral coefficients (MFCCs) to transform each audio sample into a size of $20 \times 20 \times 1$. The dataset is partitioned into 60% for training, 10% for validation and 30% for testing. The testing set is only used to evaluate the model after the training is finished. This ensures consistent and reproducible evaluation for our experiments in this study.

4.2 Implementation Details

BraTS2018: For the BraTS2018 dataset experiments, we utilized the 3D UNet architecture as the backbone network, which incorporates 3D convolutions and

⁵ Online evaluation available at <https://ipp.cbica.upenn.edu/>.

⁶ For additional data information, please refer to <https://github.com/Jakobovski/free-spoken-digit-dataset>.

⁷ The code repository can be accessed at <https://github.com/mengmenm/SMIL>.

normalization. Following a standard setup [7,10,14,38], the knowledge distillation process of cross-modal features occurs at the bottom of the UNet structure.

To optimize the network, we employed a stochastic gradient descent optimizer with Nesterov momentum [5] set at 0.99. The learning rate was initialized to 10^{-2} and gradually decreased using the cosine annealing strategy [23]. For the optimization of CKD weights, we adopt Adam optimizer with 10^{-2} as learning rate and 5×10^{-5} as the weight decay. Network parameters and CKD weights are randomly initialized. We follow the non-dedicated training setting of existing methods [7,38,45], where we randomly dropped 0 to 3 modalities to simulate missing-modality scenarios.

The model underwent 115,000 training iterations using the entire training data without model selection. The meta-validation process is conducted every 100 iterations while training. As for our CKD loss in Eq. (5), we chose $p = 1$ to form an L1 loss. For optimization in Eq. (4), we set the hyper-parameter $\alpha = 0.1$. After training, we performed the official online evaluation using the segmentation masks generated by MCKD.

Audiovision-MNIST: In the case of model training on the Audiovision-MNIST dataset, we followed the methodology outlined in the SMIL paper [25]. More specifically, the image and sound encoders used by SMIL consist of networks with a sequence of convolutional layers and fully connected (FC) layers along with batch normalization and dropout. For the remaining model architecture, after fusing the two modality features, 2 FC layers with dropout were adopted for classification. The features for the CKD loss in Eq. (5) are extracted from the layer just before the FC layers.

To optimize the model, we used the Adam optimizer with a weight decay of 10^{-2} and an initial learning rate of 10^{-3} , which was decayed by 10% every 20 epochs. To optimize the importance weight vector, we utilize the Adam optimizer with learning rate set to 10^{-2} , and weight decay set to 10^{-2} . To keep a fair comparison, we train all models (including compared models and the proposed model) for 60 epochs and drop a certain percentage of the sound modality.

To evaluate the model performance, we employed the Dice score for BraTS2018, and classification accuracy for Audiovision-MNIST. All training and evaluation procedures were conducted on a single 3090Ti NVIDIA Graphics Card.

4.3 Model Performance on Segmentation

Table 1 presents the overall performance for all 15 possible combinations of missing modalities during testing for segmenting the three sub-regions of brain tumors from BraTS2018. We compare our models with several competing models, including U-HeMIS (abbreviated as HMIS in the table) [14], U-HVED (HVED) [10], Robust-MSeg (RSeg) [7], mmFormer (mmFm) [45] and ShaSpec (ShSpec) [38]. Notably, when T1c is available, all models exhibit superior performance for the enhancing tumor (ET) segmentation compared to other modalities. Similarly, T1c for the tumor core (TC) and Flair for the whole tumor (WT) show superior results compared to other modalities, thereby validating our motivation for

Table 1: Model performance comparison on the test set of **segmentation** Dice score (in %) on BraTS2018 of **non-dedicated training**. Our models are compared with U-HeMIS (HMIS) [14], U-HVED (HVED) [10], Robust-MSeg (RbSeg) [7], mmFormer (mmFm) [45] and ShaSpec (ShSpc) [38]. ‘‘Imprv’’ denotes the improvement (in percentage) between our proposed MCKD model and the best of all other models. The best and second best results for each column within a certain type of tumor are in **bold** and *Italic*, respectively.

Modalities	Enhancing Tumor							Tumor Core							Whole Tumor									
	Fl	T1	T1c	T2	HMIS	HVED	RbSeg	mmFm	ShSpc	MCKD	Imprv	HMIS	HVED	RbSeg	mmFm	ShSpc	MCKD	Imprv	HMIS	HVED	RbSeg	mmFm	ShSpc	MCKD
•	•	•	•	11.78	23.80	25.69	39.33	<i>43.53</i>	47.37	8.85%	26.06	57.90	53.57	61.21	<i>69.44</i>	73.01	5.14%	52.48	84.39	85.69	86.10	<i>88.68</i>	89.11	0.48%
•	•	•	•	10.16	8.60	17.29	32.53	<i>41.00</i>	44.94	9.60%	37.39	33.90	47.90	56.55	<i>63.18</i>	67.16	6.30%	57.62	49.51	70.11	67.52	<i>73.44</i>	77.47	5.49%
•	•	•	•	62.02	57.64	67.07	72.60	<i>73.29</i>	76.22	4.00%	65.29	59.59	76.83	75.41	<i>78.65</i>	81.98	4.12%	61.53	53.62	73.31	72.22	<i>73.82</i>	77.72	5.28%
•	•	•	•	25.63	22.82	28.97	43.05	<i>46.31</i>	46.93	1.34%	57.20	54.67	57.49	64.20	<i>69.03</i>	69.72	1.00%	80.96	79.83	82.24	81.15	<i>83.99</i>	84.44	0.54%
•	•	•	•	10.71	27.96	32.13	42.96	<i>44.76</i>	49.64	10.90%	41.12	61.14	60.68	65.91	<i>72.67</i>	75.66	4.11%	64.62	85.71	88.24	87.06	<i>89.76</i>	90.23	0.52%
•	•	•	•	30.22	68.36	70.30	75.07	<i>75.60</i>	77.49	2.50%	71.49	75.07	80.62	77.88	<i>84.50</i>	84.82	0.38%	68.99	85.93	88.51	87.30	<i>90.06</i>	90.30	0.27%
•	•	•	•	66.10	32.31	33.84	<i>47.52</i>	47.20	50.27	5.79%	57.68	62.70	61.16	69.75	<i>72.93</i>	75.88	4.04%	82.95	87.58	88.28	87.59	<i>90.02</i>	90.39	0.41%
•	•	•	•	66.22	61.11	69.06	74.04	75.76	<i>75.41</i>	-0.46%	72.46	67.55	78.72	78.59	82.10	<i>87.85</i>	-0.30%	68.47	64.22	77.18	74.42	<i>78.74</i>	80.59	2.35%
•	•	•	•	32.39	24.29	32.01	44.99	<i>46.84</i>	49.77	4.12%	60.92	56.26	62.19	69.42	<i>71.38</i>	74.40	4.23%	82.41	81.56	84.78	82.20	<i>86.03</i>	87.05	1.19%
•	•	•	•	67.83	67.83	69.71	74.51	<i>75.93</i>	78.24	3.02%	76.64	73.92	80.20	78.61	<i>83.82</i>	84.84	1.22%	82.48	81.32	85.19	82.99	<i>85.42</i>	86.18	0.89%
•	•	•	•	68.54	68.60	70.78	75.47	<i>76.43</i>	77.66	1.62%	76.01	77.05	81.06	79.80	<i>85.23</i>	85.36	0.15%	72.31	86.72	88.73	87.33	<i>90.29</i>	90.70	0.45%
•	•	•	•	31.07	32.34	36.41	<i>47.70</i>	46.55	51.05	7.02%	60.32	63.14	64.38	71.52	<i>73.97</i>	76.73	3.73%	83.43	88.07	88.81	87.75	<i>90.36</i>	90.59	0.25%
•	•	•	•	68.72	68.93	70.88	<i>75.67</i>	75.99	75.58	-0.54%	77.53	76.75	80.72	79.55	85.26	<i>85.08</i>	-0.21%	83.85	88.09	89.27	88.14	<i>90.78</i>	90.87	0.10%
•	•	•	•	69.92	67.75	70.10	74.75	76.37	<i>75.87</i>	-0.65%	78.96	75.28	80.33	80.39	<i>84.18</i>	84.57	0.46%	83.94	82.32	86.01	82.71	<i>86.47</i>	86.94	0.54%
•	•	•	•	70.24	69.03	71.13	77.61	<i>78.08</i>	79.74	2.13%	79.48	77.71	80.86	85.78	85.45	86.20	0.49%	84.74	88.46	89.45	89.64	<i>90.88</i>	90.92	0.04%
Average	46.10	46.76	51.02	59.85	<i>61.58</i>	63.74	3.51%	62.57	64.84	69.78	72.97	<i>77.45</i>	79.15	2.19%	74.05	79.16	84.39	82.94	<i>85.92</i>	86.90	1.14%			
p-value	3.5e-6	2.2e-7	7.3e-7	6.2e-5	7.3e-5	N/A	N/A	1.6e-5	9.7e-8	4.2e-6	1.0e-7	1.8e-4	N/A	N/A	3.8e-5	6.7e-4	6.3e-6	4.5e-7	3.2e-3	N/A	N/A			

distilling the knowledge from the most informative modalities in multi-modal learning.

Our MCKD model demonstrates significant superiority over U-HeMIS, U-HVED, Robust-MSeg, mmFormer and ShaSpec in terms of segmentation Dice for whole tumor in all 15 combinations. For enhancing tumor and tumor core, it shows the best performance in 12 and 13 out of 15 combinations, respectively. Using the average results for the models, we compute the one-tailed paired t-test results for each sub-task, as shown in the last row of Table 1, and results confirm the superiority of MCKD. On average, the proposed MCKD model outperforms the state-of-the-art performance by 3.51% for enhancing tumor, 2.19% for tumor core, and 1.14% for whole tumor in terms of the segmentation Dice score.

It is worth noting that in some combinations where the best modality is missing, such as ET/TC without T1c and WT without Flair, the MCKD model exhibits a remarkable performance improvement. For instance, compared with the second best model, the ET segmentation shows a 8.85% improvement when using only the Flair modality; 9.60% improvement when using only the T1 modality; and a striking 10.90% improvement when using Flair and T1 modalities. For TC segmentation, it achieves 5.14% and 6.30% improvement with respect to the second best model, when using only Flair and T1, respectively. Similarly, for WT segmentation, it achieves 5.49% and 5.28% improvement with respect to the second best model, when using only T1 and T1c, respectively. These outstanding results confirm that the MCKD model can distill valuable knowledge from the best modalities when training the model for multi-modal learning with missing modalities.

Table 2: Model performance comparison of testing classification accuracy (in %) of missing audio (2a) and visual (2b) modalities (by setting different available audio and visual rates) on Audiovision-MNIST dataset. The lower bound (LowerB) is a LeNet [17] network trained with single modality, i.e., images only in (2a) and audio only in (2b). The upper bound (UpperB) is a model trained with all data modalities (all images and audios). The best result for each row are bolded.

Audio rate	LowerB	UpperB	AutoEncoder	GAN	Full2miss	SMIL	ShaSpec	MCKD
5%	92.35	98.22	89.78	89.11	90.00	92.89	93.33	93.56
10%	92.35	98.22	89.33	89.78	91.11	93.11	93.56	94.22
15%	92.35	98.22	89.78	88.67	92.23	93.33	93.78	94.89
20%	92.35	98.22	88.89	89.56	92.67	94.44	94.67	95.11

(a) Missing audio data.

(b) Missing visual data.

4.4 Model Performance on Classification

In line with the SMIL setup [25], we conduct the training of MCKD on both partial and full modality sub-datasets, comprising images and audios. Specifically in Tab. 2a, we create the missing modality sub-dataset by setting the audio modality rates to $\{5\%, 10\%, 15\%, 20\%\}$, which determines the proportion of available audio data used for training. In this missing audio setup, the visual modality data is fully available for training and testing. Similarly, in Tab. 2b, we set the visual modality rates to $\{5\%, 10\%, 15\%, 20\%\}$, which is the percentage of available visual data for training. In this missing visual data setup, the audio modality data is fully available for training and testing.

During the evaluation phase, only images are provided as input to the models in Tab. 2a, and only audio data is provided as input to the models in Tab. 2b. To assess the performance of MCKD, we compare it against several other models, including Auto-encoder [4], a Generative Adversarial Network (GAN) based model [12], a method for distilling multi-modality knowledge to train missing modality models [34], SMIL [25] and ShaSpec [38]. We set a LeNet [17] network with single modality (images only) as the lower bound for testing, while a model trained with full modalities (including all images and audios) serves as the upper bound for testing. For the missing visual data experiment, we only compare MCKD with SMIL and ShaSpec because they are the most accurate models and they also have code available.

As depicted in Tab. 2a, MCKD exhibits strong performance, achieving an accuracy of 94.22% compared to the second-best model with 93.56% at audio rate of 10%, and 94.89% vs. 93.78% at audio rate of 15%. Notably, as the audio rate increases, the performance of all models improves, with MCKD consistently outperforming all other models. Similarly, in Tab. 2b, MCKD improves by around 0.5% at visual rates of 5% and 10% compared to the second-best models, and with increasing visual rate, accuracy also improves for all models, where MCKD is consistently better. This can be attributed to MCKD’s exceptional ability to retain information-rich representations from important modalities and effectively use the available features to compensate for the missing modalities. Another interesting observation is that the gains from $\approx 1\%$ to $\approx 3\%$ in Tab. 2a from LowerB

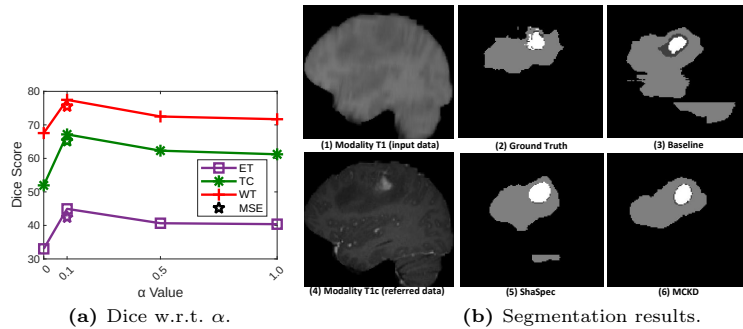


Fig. 3: In (a), we show Dice as function of α on BraTS2018 dataset with T1 modality only for testing, representing the L1 loss in Eq. 5 for $\ell_{ckd}(\cdot)$. The Dice scores obtained using the L2 loss for $\ell_{ckd}(\cdot)$ ($\alpha = 0.1$) are marked with star symbols (MSE). Different tumor regions are represented by distinct colors. In (b), we show the segmentation results produced by different models using T1 only as input for testing on BraTS2018. The images in (1) and (4) represent the MRI T1 (input data for the model) and T1c modalities (referred data, not used by the model), respectively. The “Baseline” model (3) refers to MCKD without the CKD process, while the results for ShaSpec [38] and our MCKD are shown in (5) and (6). White, dark gray and light gray correspond to distinct ET, TC and WT tumor sub-regions, respectively.

(model trained with visual data only) are much smaller than the gains of $\approx 4\%$ to $\approx 8\%$ in Tab. 2b from LowerB (model trained with audio data only). This suggests that the visual data is more important than the audio data because the improvements in Tab. 2b (when audio data is distilling the knowledge from the missing visual data) are more remarkable than the improvements in Tab. 2a (when visual data is distilling the knowledge from the missing audio data).

4.5 Analysis of MCKD

In this section, we first provide a sensitivity analysis of α in Eq. (4) and the different loss functions for $\ell_{ckd}(\cdot)$ in Eq. (5). We then show how the importance weight vectors (IWV) vary during training. We also provide visualization results of multi-modal segmentation (on BraTS2018) with missing modalities, where we compare the results with baseline methods consisting of MCKD without the cross-modal knowledge distillation (CKD) from Eq. (5), and results by ShaSpec [38] and the proposed MCKD. We conclude the section with a study on the effectiveness of our generated features, as explained in Eq. (2).

Sensitivity Analysis of α and Different Loss Functions for $\ell_{ckd}(\cdot)$ In Fig. 3a, we vary the value of α of Eq. (4), utilizing solely the T1 input for testing and applying the L1 loss for $\ell_{ckd}(\cdot)$ in Eq. (5). Notably, a dramatic drop in model performance is observed when α equals 0. However, positive values of α lead to performance improvements, with the optimal result achieved at $\alpha = 0.1$. To

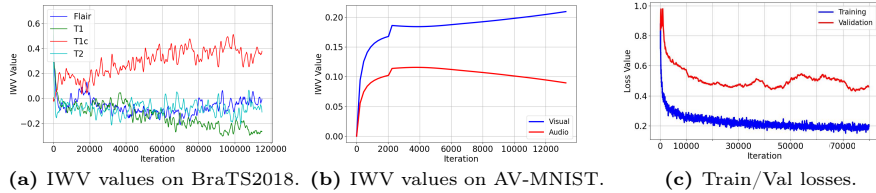


Fig. 4: Modality IWV weights changes over training iterations on BraTS2018 dataset (a) and AudioVision-MNIST (b). In (c), we have the training and validation segmentation losses on BraTS2018.

investigate the impact of a different p-norm for the CKD loss $\ell_{cka}(\cdot)$ in Eq. (5), we evaluate the Dice score using the L2 distance as the metric (i.e., MSE loss), while keeping α fixed at 0.1. A comparison between the L1 and MSE losses reveals a slight reduction in Dice score with the MSE loss over three types of tumors, showing that the L1 loss is a better option.

Visualization The segmentation visualization of different models on BraTS2018 dataset is shown in Fig. 6. As shown in the figure, the Baseline model, consisting of our MCKD without cross-modal knowledge distillation (CKD), makes many mistakes compared to ShaSpec [38] and our MCKD. Compared to ShaSpec model, despite both models having a gap to improve when using T1 modality only, MCKD shows better results, especially in the tumor boundary. This is because our MCKD is able to retain valuable cross-modal knowledge from the important modalities (e.g., T1c) when only the T1 modality is available.

The Optimization of IWV The progress of IWV during training is displayed in Figures 4a and 4b. The optimization and changes of IWV weights corresponding to different modalities are denoted using curves with different colors. By normalizing the IWV weight vector with a softmax activation function, as explained in Eq. (6), we guarantee that the sum of each element within the IWV weight vector equals to 1, which ensures that the relative importance of the modalities are kept, where changes in the weight of one element will affect the weights in other elements. In our training, at least one modality will dominate the others, and consequently receive a high IWV weight. This large IWV weight modality will then be used by other modalities in a knowledge distillation process. As shown in Figure 4a, the IWV weight of T1c (in red) is above other curves, showing the significance of the modality T1c for Brain Tumor detection (particularly for enhancing tumor and tumor core). This observation resonates with the fact that enhancing tumor and tumor core is clearly visible in T1c [7]. Interestingly, we also notice that the IWV weight of Flair (in dark blue) is smaller than the weight for T1c, but it has a sharp increase at around 10000 iterations, suggesting the importance of this modality at that training stage. After that, the Flair weight decreases and becomes similar to the weights of T1 and T2, but

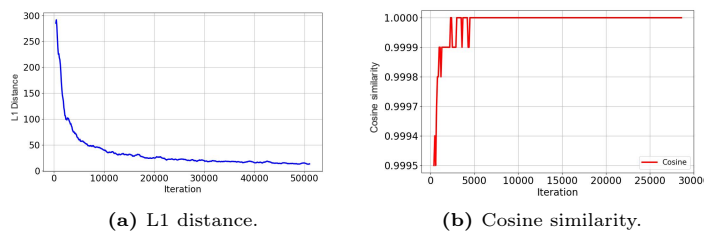


Fig. 5: L1 distance (a) and cosine similarity (b) between generated features and missing features from T1c, when it is unavailable, over training iterations on BraTS2018.

still slightly higher than them at the end of the training. This phenomenon may be attributed to the effective distillation of Flair features at the beginning of the optimization (particularly for the whole tumor); then the model subsequently prioritizes the distillation of T1c features. This pattern also holds for AudioVision classification shown by Fig. 4b. It shows the visual modality receives higher importance gradually than the audio modality. An important question is if our training dynamics leads to the overfitting of the dominant modality. However, the training and validation losses shown in Fig. 4c suggest that such training dynamics does not result in overfitting.

Examining the Generation of Missing Features One potential question about our MCKD is its ability to generate appropriate features for the missing modalities with the technique in Eq. (2). To test that, we show in Figure 5a and Figure 5b, the L1 distance and Cosine Similarity, respectively, between the generated feature from Eq. (2) and the actual feature from the missing T1c modality as training progresses. Note that distance decreases and similarity goes up steadily with training iterations, which is critical for the functionality of MCKD.

5 Conclusion

In this paper, we address the model performance drop problem for multi-modal learning methods when top-performing modalities are missing. In particular, we introduce a novel approach, named MCKD, which aims to solve this challenge with a meta-learning optimization that dynamically optimizes the importance of each modality and conducts a cross-modal knowledge distillation to transfer knowledge from high-informative to low-informative modalities. The resulting model shows promising performance, even when influential modalities are missing. On BraTS2018 dataset, the proposed MCKD showcases significant improvements over recently published models, with average segmentation Dice score enhancements of 3.51% for enhancing tumors, 2.19% for tumor cores, and 1.14% for whole tumors. Extensive analyses further verify the effectiveness of the learned IWW weights to identify important modalities.

One potential weakness of our method is the simplistic missing modality feature generation procedure in Eq. (2) that consists of the mean feature from the image modalities present in the input. Even though this consists of a simple feature generation approach, we show in Fig. 5a and Fig. 5b that it is quite effective at producing useful features for the training of MCKD. Nevertheless, we plan to integrate more powerful feature generation procedures based on generative models, such as conditional generative models [27, 35].

References

1. Albanie, S., Nagrani, A., Vedaldi, A., Zisserman, A.: Emotion recognition in speech using cross-modal transfer in the wild. In: Proceedings of the 26th ACM international conference on Multimedia. pp. 292–301 (2018) 4
2. Azad, R., Khosravi, N., Merhof, D.: Smu-net: Style matching u-net for brain tumor segmentation with missing modalities. In: International Conference on Medical Imaging with Deep Learning. pp. 48–62. PMLR (2022) 4
3. Bakas, S., Reyes, M., Jakab, A., Bauer, S., Rempfler, M., Crimi, A., Shinohara, R.T., Berger, C., Ha, S.M., Rozycki, M., et al.: Identifying the best machine learning algorithms for brain tumor segmentation, progression assessment, and overall survival prediction in the brats challenge. arXiv preprint arXiv:1811.02629 (2018) 6, 7
4. Baldi, P.: Autoencoders, unsupervised learning, and deep architectures. In: Proceedings of ICML workshop on unsupervised and transfer learning. pp. 37–49. JMLR Workshop and Conference Proceedings (2012) 11
5. Botev, A., Lever, G., Barber, D.: Nesterov’s accelerated gradient and momentum as approximations to regularised update descent. In: 2017 International Joint Conference on Neural Networks (IJCNN). pp. 1899–1903. IEEE (2017) 9
6. Chartsias, A., Joyce, T., Giuffrida, M.V., Tsaftaris, S.A.: Multimodal mr synthesis via modality-invariant latent representation. IEEE transactions on medical imaging 37(3), 803–814 (2017) 4
7. Chen, C., Dou, Q., Jin, Y., Chen, H., Qin, J., Heng, P.A.: Robust multimodal brain tumor segmentation via feature disentanglement and gated fusion. In: International Conference on Medical Image Computing and Computer-Assisted Intervention. pp. 447–456. Springer (2019) 2, 4, 9, 10, 13
8. Chen, H., Xie, W., Afouras, T., Nagrani, A., Vedaldi, A., Zisserman, A.: Localizing visual sounds the hard way. In: Proceedings of the IEEE/CVF Conference on Computer Vision and Pattern Recognition. pp. 16867–16876 (2021) 4
9. Chen, Y., Pan, Y., Xia, Y., Yuan, Y.: Disentangle first, then distill: A unified framework for missing modality imputation and alzheimer’s disease diagnosis. IEEE Transactions on Medical Imaging (2023) 4
10. Dorent, R., Joutard, S., Modat, M., Ourselin, S., Vercauteren, T.: Hetero-modal variational encoder-decoder for joint modality completion and segmentation. In: International Conference on Medical Image Computing and Computer-Assisted Intervention. pp. 74–82. Springer (2019) 2, 4, 9, 10
11. Dou, Q., Liu, Q., Heng, P.A., Glocker, B.: Unpaired multi-modal segmentation via knowledge distillation. In: IEEE Transactions on Medical Imaging (2020) 3
12. Goodfellow, I., Pouget-Abadie, J., Mirza, M., Xu, B., Warde-Farley, D., Ozair, S., Courville, A., Bengio, Y.: Generative adversarial networks. Communications of the ACM 63(11), 139–144 (2020) 11

13. Han, Z., Zhang, C., Fu, H., Zhou, J.T.: Trusted multi-view classification. arXiv preprint arXiv:2102.02051 (2021) [3](#)
14. Havaei, M., Guizard, N., Chapados, N., Bengio, Y.: Hemis: Hetero-modal image segmentation. In: International Conference on Medical Image Computing and Computer-Assisted Intervention. pp. 469–477. Springer (2016) [2](#), [4](#), [9](#), [10](#)
15. Hu, M., Maillard, M., Zhang, Y., Ciceri, T., La Barbera, G., Bloch, I., Gori, P.: Knowledge distillation from multi-modal to mono-modal segmentation networks. In: International Conference on Medical Image Computing and Computer-Assisted Intervention. pp. 772–781. Springer (2020) [4](#)
16. Jia, X., Jing, X.Y., Zhu, X., Chen, S., Du, B., Cai, Z., He, Z., Yue, D.: Semi-supervised multi-view deep discriminant representation learning. IEEE transactions on pattern analysis and machine intelligence **43**(7), 2496–2509 (2020) [4](#)
17. LeCun, Y., Bottou, L., Bengio, Y., Haffner, P.: Gradient-based learning applied to document recognition. Proceedings of the IEEE **86**(11), 2278–2324 (1998) [8](#), [11](#)
18. Lee, H.Y., Tseng, H.Y., Huang, J.B., Singh, M., Yang, M.H.: Diverse image-to-image translation via disentangled representations. In: Proceedings of the European conference on computer vision (ECCV). pp. 35–51 (2018) [4](#)
19. Lee, Y.L., Tsai, Y.H., Chiu, W.C., Lee, C.Y.: Multimodal prompting with missing modalities for visual recognition. In: Proceedings of the IEEE/CVF Conference on Computer Vision and Pattern Recognition. pp. 14943–14952 (2023) [4](#)
20. Lin, R., Hu, H.: Missmodal: Increasing robustness to missing modality in multimodal sentiment analysis. Transactions of the Association for Computational Linguistics **11**, 1686–1702 (2023) [4](#)
21. Liu, J., Capurro, D., Nguyen, A., Verspoor, K.: Attention-based multimodal fusion with contrast for robust clinical prediction in the face of missing modalities. Journal of Biomedical Informatics **145**, 104466 (2023) [4](#)
22. Liu, X., Sanchez, P., Thermos, S., O’Neil, A.Q., Tsaftaris, S.A.: Learning disentangled representations in the imaging domain. Medical Image Analysis p. 102516 (2022) [4](#)
23. Loshchilov, I., Hutter, F.: Sgdr: Stochastic gradient descent with warm restarts. arXiv preprint arXiv:1608.03983 (2016) [9](#)
24. Ma, M., Ren, J., Zhao, L., Testuggine, D., Peng, X.: Are multimodal transformers robust to missing modality? In: Proceedings of the IEEE/CVF Conference on Computer Vision and Pattern Recognition. pp. 18177–18186 (2022) [4](#)
25. Ma, M., Ren, J., Zhao, L., Tulyakov, S., Wu, C., Peng, X.: Smil: Multimodal learning with severely missing modality. In: Proceedings of the AAAI Conference on Artificial Intelligence. vol. 35, pp. 2302–2310 (2021) [2](#), [4](#), [8](#), [9](#), [11](#)
26. Menze, B.H., Jakab, A., Bauer, S., Kalpathy-Cramer, J., Farahani, K., Kirby, J., Burren, Y., Porz, N., Slotboom, J., Wiest, R., et al.: The multimodal brain tumor image segmentation benchmark (brats). IEEE transactions on medical imaging **34**(10), 1993–2024 (2014) [6](#), [7](#)
27. Mirza, M., Osindero, S.: Conditional generative adversarial nets. arXiv preprint arXiv:1411.1784 (2014) [15](#)
28. Monteiro, M., Le Folgoc, L., Coelho de Castro, D., Pawlowski, N., Marques, B., Kamnitsas, K., van der Wilk, M., Glocker, B.: Stochastic segmentation networks: Modelling spatially correlated aleatoric uncertainty. Advances in Neural Information Processing Systems **33**, 12756–12767 (2020) [3](#)
29. Nair, V., Hinton, G.E.: Rectified linear units improve restricted boltzmann machines. In: Proceedings of the 27th international conference on machine learning (ICML-10). pp. 807–814 (2010) [18](#)

30. OpenAI: Gpt-4 technical report (2023) [2](#)
31. Patrick, M., Asano, Y.M., Kuznetsova, P., Fong, R., Henriques, J.F., Zweig, G., Vedaldi, A.: Multi-modal self-supervision from generalized data transformations. arXiv preprint arXiv:2003.04298 (2020) [4](#)
32. Patrick, M., Huang, P.Y., Misra, I., Metze, F., Vedaldi, A., Asano, Y.M., Henriques, J.F.: Space-time crop & attend: Improving cross-modal video representation learning. In: Proceedings of the IEEE/CVF International Conference on Computer Vision. pp. 10560–10572 (2021) [4](#)
33. Prakash, A., Chitta, K., Geiger, A.: Multi-modal fusion transformer for end-to-end autonomous driving. In: Proceedings of the IEEE/CVF Conference on Computer Vision and Pattern Recognition. pp. 7077–7087 (2021) [2](#)
34. Shen, Y., Gao, M.: Brain tumor segmentation on mri with missing modalities. In: International Conference on Information Processing in Medical Imaging. pp. 417–428. Springer (2019) [2](#), [4](#), [11](#)
35. Sohn, K., Lee, H., Yan, X.: Learning structured output representation using deep conditional generative models. Advances in neural information processing systems **28** (2015) [15](#)
36. van Tulder, G., de Bruijne, M.: Learning cross-modality representations from multi-modal images. IEEE transactions on medical imaging **38**(2), 638–648 (2018) [4](#)
37. Vielzeuf, V., Lechervy, A., Pateux, S., Jurie, F.: Centralnet: a multilayer approach for multimodal fusion. In: Proceedings of the European Conference on Computer Vision (ECCV) Workshops. pp. 0–0 (2018) [8](#)
38. Wang, H., Chen, Y., Ma, C., Avery, J., Hull, L., Carneiro, G.: Multi-modal learning with missing modality via shared-specific feature modelling. In: Proceedings of the IEEE/CVF Conference on Computer Vision and Pattern Recognition. pp. 15878–15887 (2023) [2](#), [4](#), [9](#), [10](#), [11](#), [12](#), [13](#), [18](#)
39. Wang, H., Wu, Q., Shen, C.: Soft expert reward learning for vision-and-language navigation. In: European Conference on Computer Vision. pp. 126–141. Springer (2020) [2](#)
40. Wang, H., Zhang, J., Chen, Y., Ma, C., Avery, J., Hull, L., Carneiro, G.: Uncertainty-aware multi-modal learning via cross-modal random network prediction. arXiv preprint arXiv:2207.10851 (2022) [2](#), [4](#)
41. Wang, Y., Huang, W., Sun, F., Xu, T., Rong, Y., Huang, J.: Deep multimodal fusion by channel exchanging. Advances in Neural Information Processing Systems **33**, 4835–4845 (2020) [4](#)
42. Wang, Y., Zhang, Y., Liu, Y., Lin, Z., Tian, J., Zhong, C., Shi, Z., Fan, J., He, Z.: Acn: Adversarial co-training network for brain tumor segmentation with missing modalities. In: International Conference on Medical Image Computing and Computer-Assisted Intervention. pp. 410–420. Springer (2021) [2](#), [4](#)
43. Yang, H., Sun, J., Xu, Z.: Learning unified hyper-network for multi-modal mr image synthesis and tumor segmentation with missing modalities. IEEE Transactions on Medical Imaging (2023) [4](#)
44. Yin, Q., Wu, S., Wang, L.: Unified subspace learning for incomplete and unlabeled multi-view data. Pattern Recognition **67**, 313–327 (2017) [2](#), [4](#)
45. Zhang, Y., He, N., Yang, J., Li, Y., Wei, D., Huang, Y., Zhang, Y., He, Z., Zheng, Y.: mmformer: Multimodal medical transformer for incomplete multimodal learning of brain tumor segmentation. arXiv preprint arXiv:2206.02425 (2022) [4](#), [9](#), [10](#)
46. Zhou, T., Canu, S., Vera, P., Ruan, S.: Feature-enhanced generation and multi-modality fusion based deep neural network for brain tumor segmentation with missing mr modalities. Neurocomputing **466**, 102–112 (2021) [4](#)

6 Appendix

6.1 Normalization Functions for Eq. (6)

We tried different IWV normalization functions in Eq. (6), with results in Table 3. Note that the softmax normalization leads to the best results.

Normalization	Enhancing Tumor	Tumor Core	Whole Tumor
ReLU(\cdot)	71.20	81.99	90.31
Sigmoid(\cdot)	73.99	80.18	87.74
Softmax(\cdot)	77.66	85.36	90.70

Table 3: Segmentation Dice scores (in %) to experiment with different normalization functions, including ReLU [29], Sigmoid function and Softmax function, adopted for IWV learning in Eq. (6), using Flair, T1 and T1c for testing on BraTS2018.

6.2 More Visualizations

We provide additional segmentation results of different models on BraTS2018 dataset. In Figures 6 and 7, we show the segmentation results produced by different models using T1 only as input for testing on BraTS2018. The images in (a) and (d) represent the MRI T1 (input data for the model) and T1c modalities (referred data, not used by the model), respectively. The “Baseline” model (c) refers to MCKD without the CKD process, while the results for ShaSpec [38] and our MCKD are shown in (e) and (f). White, dark gray and light gray correspond to distinct ET, TC and WT tumor sub-regions, respectively. In Figure 6, while both the baseline model and ShaSpec exhibited shortcomings in detecting the ET tumor (in white), MCKD demonstrates the capability of successfully identifying it. A similar situation is showed in Figure 7, where our MCKD achieves qualitatively better segmentation results on all three tumor regions, compared to the Baseline model or ShaSpec.

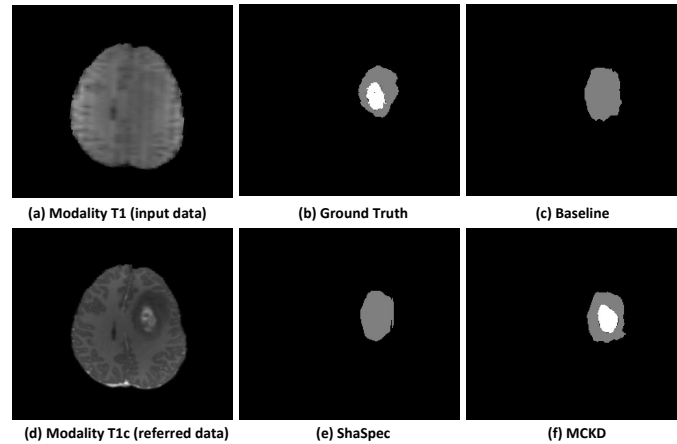


Fig. 6: Additional visualization of the segmentation results produced by different models using T1 (input data for the model) only for testing on BraTS2018. T1c serves for the referred data, which is not used by the model.

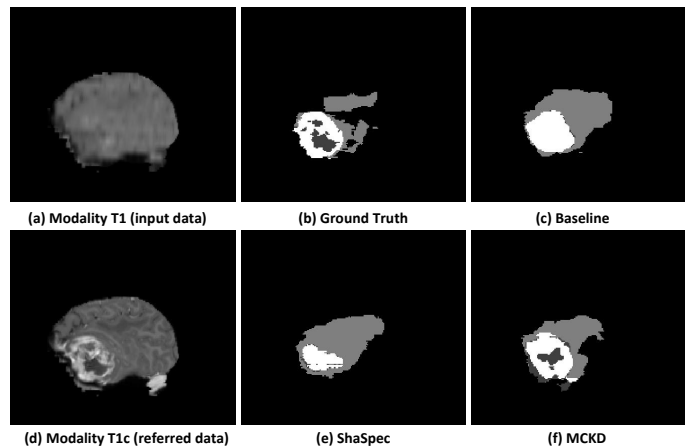


Fig. 7: Additional visualization of the segmentation results produced by different models using T1 (input data for the model) only for testing on BraTS2018. T1c serves for the referred data, which is not used by the model.